RSC Advances

ROYAL SOCIETY OF CHEMISTRY

www.rsc.org/advances

Table of contents entry

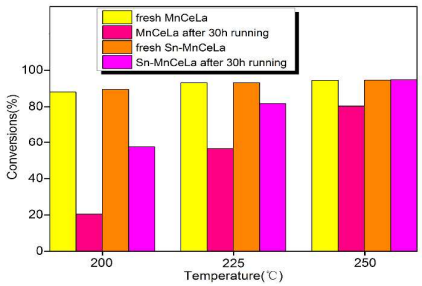

The Sn-Modified MnCeLa catalysts show significantly higher resistance to chlorine poisoning than that of MnCeLa catalysts at different temperatures.

Enhancement of resistance to chlorine poisoning of Sn-modified MnCeLa catalysts for chlorobenzene oxidation at low temperature

Dou Mao, Fei He, Pei Zhao, Shantang Liu*

Key Laboratory for Green Chemical Process of Ministry of Education, School of Chemistry and Environmental Engineering, Wuhan Institute of Technology, Wuhan 430074, China

*Corresponding Author. Tel.:+86 27 87195001; E-mail: liushantang@mail.wit.edu.cn

Abstract

In this article, MnCeLa and Sn-MnCeLa mixed oxide catalysts prepared by sol-gel and coprecipitation method were evaluated for the catalytic combustion of chlorobenzene (CB), which was employed as a model compound for volatile organic chlorinated aromatics. The activity tests revealed that both catalysts presented an excellent activity in catalytic destruction of CB showing 90% conversion below 210 °C. A considerably higher stability was observed for the Sn-MnCeLa catalyst compared with MnCeLa sample, indicating that the catalytic stability of MnCeLa catalyst for chlorobenzene oxidation could be significantly enhanced via the introduction of Sn. X-ray photoelectron Spectroscopy (XPS) demonstrated that Sn modification can increase the concentration of surface reactive oxygen species, which is critical to remove Cl species. Additionally, Raman and hydrogen temperature programmed reduction (H_2-TPR) showed that the addition of Sn inhibited the formation of MnO_xCl_y on the active sites of MnCeLa catalyst. These two aspects are responsible for the remarkably improved resistance to chlorine poisoning of Sn-Modified MnCeLa catalyst.

Key words: Sn; MnCeLa; Chlorobenzene; Chlorine removal; Catalytic combustion

1. Introduction

Chlorinated volatile organic compounds (CVOCs), due to their acute toxicity, strong odor and potential bioaccumulation are not only hazardous air pollutants,[1,2] but are also highly carcinogenic, teratogenic and mutagenic in nature.[3,4] Therefore, it is essential to develop practical and cost-effective methods to eliminate CVOCs from gases. Of the available techniques, the catalytic combustion is one of the most effective technologies for the removal of CVOCs emissions due to its low energy consumption, low processing temperature and high destructive efficiency.

Among the catalysts used for the catalytic combustion of CVOCs, manganese oxides have been reported as the most active ones on account of their high oxygen storage ability and redox properties.[5-9] Furthermore, when these Mn-based catalysts are modified by rare earth elements, such as MnO_x-CeO_2, $LaMnO_3$ and Mn-Ce-La-O catalysts, they have been found to display a higher catalytic performance in the oxidation of CVOCs in comparison with MnO_x catalysts alone.[10-13] Notably, catalysts MnCeLa are reported to present the best catalytic activity in the catalytic oxidation of CB among them. However, these oxides are susceptible to rapid catalytic deactivation due to strong adsorption of dissociative Cl species that are mainly generated from the combustion processes. Undoubtedly, any improvement in these catalysts' resistance to deactivation will extend the application range of manganese oxides in industry. To this end, some researchers attempted to remove the Cl species through desorption or oxidation by increasing the reaction temperature.[14]

SnO_2, which was employed as a catalyst support[15,16] or a promoter,[17-19] has received considerable attentions as a heterogeneous catalyst. Recently, Sn modified MnO_x-CeO_2 catalysts

have been used in the selective catalytic reduction of NO_x by NH_3 and exhibited considerably high activity and better resistance to sulfur poisoning, due to the enhanced concentration of oxygen vacancies[20] and Lewis acid sites.[21] However, as far as we know, Sn modified Mn-based catalysts for catalytic combustion of CB are rarely reported. In order to solve the problem mentioned above, in this work, we have introduced Sn into Mn-based catalysts (MnCeLa) for catalytic combustion of chlorobenzene. It was found that the Sn-MnCeLa catalysts presented excellent activity and higher stability compared to MnCeLa catalysts at low temperature region. Additionally, the possible reasons for the better stability of Sn-MnCeLa catalyst have been elucidated through several characterization techniques.

2. Experimental

2.1 Catalysts preparation

Sn-MnCeLa mixed oxides were prepared by sol-gel and coprecipitation method, as follows: In the first step, an aqueous solution containing $Mn(NO_3)_2$ (50 wt.% solution), $Ce(NO_3)_3 \cdot 6H_2O$ (SCRC, 99.0%), $La(NO_3)_3 \cdot 6H_2O$ (SCRC, 99.0%) and citric acid (SCRC, 99.0%, citric acid/(Mn/1.5 + Ce + La + Sn) = 0.3, molar ratio) (in the solution, Mn/(Ce + La) = 12:1, Ce/La = 1:1, molar ratio) was gradually heated to 80 ℃ and kept at this temperature with stirring until the color of the solution turned yellowish. It was then dried at 110 ℃ for 12 h. In the second step, the resulting solid mass was added to a $SnCl_2 \cdot 2H_2O$ solution (SCRC, 98.0%, Sn/(Sn + Mn + Ce + La) = 0.08:1, molar ratio) and then the PH was adjusted to 9~10 with $NH_3 \cdot H_2O$ and kept for aging overnight. On filtration, a precipitate was obtained which was washed with deionized water until no chloride ion was detected. The obtained solid was dried overnight at 110 ℃, followed by calcination at 650 ℃ in a muffle furnace for 5 h under air. The same method was employed to

prepare MnCeLa, MnLa, MnCe and LaCe catalysts. The compositions of the reaction solution and calcination temperature were the same as those in the aforementioned procedure. The synthesized catalysts are denoted as MnCeLa and Sn-MnCeLa, respectively. Sometimes, Sn(x)-MnCeLa can also be abbreviated as Sn(x), where x represents the molar ratio for Sn/(Sn + Mn + Ce + La), e.g. Sn(0.08).

2.2 Characterization

The phase structure of catalyst was recorded on an X'Pert PW3050/60 X-ray diffractometer with Cu Kα radiation (40 kV and 40 mA). The Raman spectra were analyzed by a laser confocal microscopy Raman spectrometer (DXR, American Thermo Electron) operated at a wavelength of 532 nm. The nitrogen adsorption and desorption isotherms were measured on Micromeritics ASAP 2020 nitrogen-adsorption apparatus. The specific surface areas of samples were measured using Brunauer-Emmett-Teller (BET) model, and the pore volume and pore size distributions were calculated by Barrett-Jioner-Halenda (BJH) method. X-ray photoelectron spectroscopy with Al Kα X-ray (hυ=1253.6 eV) radiation (XPS: VG Multilab 2000) was used to analyze the surface atomic states of the catalysts. The H_2-temperature programming reduction (H_2-TPR) was investigated by heating catalysts with a linear heating rate (10 °C/min) in a flow of 10% H_2 in argon with a flow rate of 40 mL/min. The rate of hydrogen consumption was measured by a thermal conductivity detector (TCD).

2.3 Catalytic activity test

The activity of the catalysts was measured at atmospheric pressure, under continuous flowing air, in a micro reactor with an inner diameter of 8 mm, in which 0.2 g of the catalyst was placed at

the center. Chlorobenzene was introduced into the reactor by N_2 (carrying gas), flowing through a saturator maintained at 0 °C, and then mixed with N_2 and O_2 in a mixing drum. The feed stream through the reactor was prepared by delivering liquid chlorobenzene with concentration of CB 2500 mg/m^3 and the gas hourly space velocity (GHSV) was maintained at 20,000 h^{-1}. The conversion of the chlorobenzene by the catalyst was expressed as the activity of the catalyst. The temperature of the reaction was measured and controlled with a thermocouple located just at the thermal spot of the reactor. The effluent gases were analyzed at a given temperature by using an online gas chromatograph (GC) equipped with flame ionization detector (FID) for the quantitative analysis of CB. The hydrogen consumption was measured quantitatively by a thermal conductivity detector (TCD).

3.Results and discussions

3.1. Catalytic activity for CB oxidation

The activities of SnO_2, MnCeLa and Sn-MnCeLa catalysts are shown in Fig. 1. As seen in Fig S1 (Supporting Information), the conversions of CB follow the sequence: MnCeLa > MnCe > MnLa > MnO_x > La_2O_3 > LaCe > CeO_2, indicating that after modification by La and Ce, MnO_x possesses the best activity. Notably, La_2O_3 and CeO_2, acting as additives, can promote the thermal stability and redox ability of the Mn-based catalyst, respectively.[22] In comparison to SnO_2, which shows no significant oxidation of CB at temperatures up to 250 °C, the catalyst MnCeLa exhibits excellent catalytic activity showing conversions of 50% and 90% ($T_{50\%}$ and $T_{90\%}$) at 149°C and 210°C, respectively. In the case of Sn-MnCeLa catalysts, when the content of Sn is not greater than 8% (Sn/(Sn + Mn + Ce + La) = 8%, molar ratio), the activity is almost identical to that of the MnCeLa catalyst. However, on further addition of Sn, the activity of Sn-MnCeLa catalysts

decreased significantly due to the decrease of Mn amount. These results reveal that MnO_x is the main active component in the catalysts: Sn acts as an additive, and the small amount of Sn affects the activity of the catalyst barely.

3.2. Stability studies of the catalysts

For commercial applications, stability of catalysts is an important factor. Fig. 2 shows the stabilities of MnCeLa and Sn(0.08)-MnCeLa catalysts which were reacted continuously at different temperatures for 30 h. It can be seen in figures 2a, 2b and 2c that both the catalysts were deactivated to some extent at temperatures less than 250 °C. The activity of MnCeLa catalyst was not stable until 300 °C. However, for Sn(0.08)-MnCeLa, the temperature needed for stable activity was 250 °C, which was much lower than other manganese-containing catalysts,[10,23,24] noble metal catalysts[25,26] and other catalysts.[27] Moreover, compared with the MnCeLa catalyst, the deactivation rate of Sn(0.08)-MnCeLa was slower and the final stable activity was higher below 300 °C. These facts indicate that the addition of Sn resulted in an obvious enhancement in the stability of the MnCeLa catalyst. Subsequently, a series of characterizations were conducted to investigate the effect of Sn.

3.3. Catalyst characterizations

3.3.1. BET and XRD

To investigate whether the physical structures of the catalysts change during the catalytic reaction, the BET (Table 1) of the fresh and used catalysts (used catalysts refer to the most poisoned catalysts, which are reacted at 200 °C for 30 h, denoted as used MnCeLa or Sn-MnCeLa in the later text) was employed. The results indicated that the aforementioned parameters

minimally changed after the oxidation of CB for both the MnCeLa and Sn-MnCeLa catalysts, manifesting that the physical structures of catalysts do not change during the stability test. Fig. 3 presents wide angle XRD patterns of fresh and used catalysts. The diffractogram of CeO_2 shows the diffraction peaks (at 28.5°, 33.1°, 47.5°, 56.5° and 59.2°) of cerianite characterized with a fluorite-like structure (JCPDS #43-1002). For fresh samples, no obvious reflections belonging to cubic fluorite structure of CeO_2 can be observed, except for a small peak at ca. 33°, which is attributed to (2 0 0) lattice plane of cerianite. Compared to fresh MnCeLa, the diffraction peak of fresh Sn-MnCeLa become less intense and shift to higher Bragg angles, from 32.9° to 33.3°, indicating that part of Sn species can enter the fluorite lattice to form $SnCeO_x$ solid solutions.[28] This result is because that the ionic radius of Sn^{4+} (0.071nm) is smaller than that of Ce^{4+} (0.094nm), and the incorporation of Sn^{4+} into the fluorite lattice will result in the decrease in lattice parameters. These very low intensity reflections of Sn-MnCeLa catalysts confirm that the crystallinity of the samples can significantly decrease due to Sn doping,[29] which is better illustrated by the XRD patterns of different Sn amounts of Sn-MnCeLa catalysts in Fig S2 (Supporting Information).

In addition to the reflections of the cerianite, no signals corresponding to Mn species appear for the fresh and used catalysts, except for used MnCeLa sample, on which the reflections from α-Mn_2O_3 at 55.17° and 65.77° (JCPDS #24-0508) and MnO_2 at 37.05° (JCPDS #42-1169)[30] are observed. The crystalline phase corresponding to La species (49.27° and 45.18° (JCPDS #54-1275))[12] cannot observed, due to a high dispersion of La species either into or between fluorite matrix.

3.3.2. Raman

To further explore the effect of Sn on MnCeLa, Raman spectroscopy was employed. As shown in Figure 4, Raman spectra of fresh and used samples were collected for comparisons and the main characteristic peaks of pure SnO_2, MnO_x, La_2O_3 and CeO_2 were also given as contrast. For MnCeLa catalysts, no characteristic vibrational modes of CeO_2 or La_2O_3[31] are observed, except a broad peak in the region of 500-700 cm^{-1}, which can be assigned to a Mn-O-Mn stretching mode of Mn_3O_4-like species ($\nu_{Mn\text{-}O\text{-}Mn}$).[12] Combining with XRD analysis, it is reasonable to infer that the symmetry band of $\nu_{Mn\text{-}O\text{-}Mn}$ at 633 cm^{-1} can be attributed to the presence of Mn_2O_3 or MnO_2 species. After catalytic oxidation of CB, the band became broader with the intensity decreasing drastically, indicating that the vibrational mode of Mn-O-Mn became asymmetric due to the formation of Mn-O-Cl. This result demonstrated that the MnO_x species, acted as main active component, reacted with dissociative Cl species during the catalytic reaction and thus formed oxychlorinated manganese (MnO_xCl_y).[32] However, for Sn-MnCeLa, there were no apparent differences between the fresh and used samples, manifesting that the addition of Sn could inhibit the formation of MnO_xCl_y, avoiding the chlorine poisoning of the MnCeLa catalyst. As reported in Refs,[33,34] the peak at 643 cm^{-1} can be attributed to the overlapping of MnO_2 and SnO_2. In addition, compared to pure MnO_2 and SnO_2, red shift and blue shift of the peak were observed respectively, implying that there were interactions between Sn and Mn species. It is likely that Sn entered into MnO_x lattice to form $SnMnO_x$ solid solution.[35] Furthermore, compared to fresh MnCeLa sample, the band shifted to higher wavenumbers by 10 cm^{-1}, indicating that Sn modification maintained the structure of MnO_x in the form of $SnMnO_x$ solid solution during CB decomposition. Additionally, a new peak centered at ca. 450 cm^{-1} appeared by Sn doping for fresh Sn-MnCeLa catalyst. As supported by XRD results, it is reasonable to infer that the peak is attributed to

$SnCeO_x$ solid solutions. It is interesting to find that the Raman peak disappeared after CB oxidation, implying the structure of $SnCeO_x$ solid solution was destroyed by Cl species. From the analysis above, we can deduce that Cl species preferentially reacted with the $SnCeO_x$ solid solution rather than MnO_x species. In other words, $SnCeO_x$ solid solution "sacrificed" itself to maintain the high activity of MnO_x species during CB oxidation.

3.3.3. XPS

To gain better insight into the nature of the species and the surface groups of the catalysts, the catalysts were examined using XPS (see Fig. 5), and the data were summarized in Table 1. Mn species with Mn 2p levels of 640.5, 641.8 and 643.7 eV on the surface of catalysts containing Mn can be ascribed to Mn^{2+}, Mn^{3+} and Mn^{4+} ions.[36] The fitted XPS spectra of Mn 2p were shown in Fig. 5(A). From table 1, it can be seen that the atomic ratio of Mn^{4+} and Mn^{3+} in fresh Sn-MnCeLa (35.2% and 47.1%) was higher than that of fresh MnCeLa (26.2% and 39.6%), respectively. It indicated that the addition of Sn affects the oxidation state of Mn with high valence, which was more effective in the oxidation of the adsorbed chlorobenzene.[37] Therefore, the increased ratios of Mn with high valence imparted high reducibility within the catalyst, or in other words, introduced enhanced activity within the catalyst Sn-MnCeLa. As shown in Fig. 5(B), the O 1s profile mainly includes two components, 531.3−532.2 eV and 529.2−530.0 eV. The peak at the high binding energies (BE) corresponds to the surface adsorbed oxygen (O_{ads}) such as O_2^{2-} or O^- and hydroxyl OH^-, whereas that at the low BE is attributed to the lattice oxygen O^{2-} (O_{latt}).[20] For fresh samples, the ratio O_{ads} /(O_{ads} + O_{latt}) in Sn-MnCeLa (30.2%) was higher than that in MnCeLa (21.9%), implying that Sn addition can significantly increase the concentration of the surface adsorbed oxygen, which was consistent with the results of Chang and co-workers.[20] Since the surface

adsorption oxygen (O_{ads}) was active in HCl oxidation reaction (i.e., the so-called Deacon process, $4HCl + O_2 \rightarrow 2H_2O + 2Cl_2$),[38] higher the O_{ads} ratio in Sn-MnCeLa catalysts, easier was the Cl species removal from the catalysts' surface.

Figure S3 (a) (Supporting Information) represents the XPS spectra of Ce 3d in the MnCeLa and Sn-MnCeLa samples. The spectra were deconvolved into two spin-orbits, and letters U and V refer to the $3d_{3/2}$ and $3d_{5/2}$ spin-orbit components respectively. All the peaks V, V^{II}, U, U^{II} and U^{III} were attributed to Ce^{4+}.[39] The La 3d core level is shown in Figure S3 (b) (Supporting Information) and the spectrum of La $3d_{3/2}$ and La $3d_{5/2}$ appeared at ca. 850 eV and 834.1-834.0 eV,[12] respectively.

The Sn 3d XPS spectra are presented in Fig. 5(C). It is worth mentioning that the intensity of Sn^{2+} peak (485.2 eV) increased after stability test, revealing that some Sn^{4+} participated in the catalytic oxidation process and was reduced to Sn^{2+}, which was evidenced by Raman results.

As reported in Reference,[40] the Cl 2p peak appeared at around 198.3 eV. From figure 5 (D), it can be seen that the Cl species deposited on the surface of the used Sn-MnCeLa (0.71%) was lower than that on used MnCeLa (1.29%), indicating that the addition of Sn could improve the resistance to Cl poisoning and therefore promote the stability of the catalysts.

3.3.4. H_2-TPR

Fig. 6 presents the H_2-TPR results of the MnCeLa and Sn-MnCeLa catalysts. Assuming that MnO is the final reduction state[41] from various Mn species in the initial MnO_x, it is reasonable to propose that the peak at low temperature could be assigned to the reduction of MnO_2/Mn_2O_3 to Mn_3O_4, and the one at high temperature corresponds to the reduction of Mn_3O_4 to MnO.[42,43] For fresh MnCeLa catalyst, two broad overlapped reduction peaks representing the reduction of $MnO_2/Mn_2O_3 \rightarrow Mn_2O_3$ and $Mn_3O_4 \rightarrow MnO$ appeared around 312 and 371 °C, respectively. In

addition, shoulders were observed on the left side of the low reduction peaks of MnO_x around 220 °C, which were attributed to the "isolated" Mn ions with high valence state that were "embedded" within the surface defects of the catalyst.[12] Compared with fresh MnCeLa, the intensity of the low temperature reduction peaks for these used catalysts decreased, implying that the content of high valence Mn deceased after the oxidation of CB, which was consistent with the XPS results. Moreover, new shoulder peaks centered at approximately 360 °C were observed, which can be attributed to the removal of Cl species adsorbed on the surface of Mn,[29] that is, H_2 reacted with adsorbed Cl to form HCl. For MnCeLa (300 °C), the reduction temperatures of Mn shifted to lower values, this phenomenon indicated that high temperature promotes the activation of catalyst to some extent. It is noteworthy that a new broad peak centered in the region of 700-800 °C appeared for the used catalysts, especially for MnCeLa (275 °C) and MnCeLa (300 °C), which can be ascribed to the reduction of oxychlorinated manganese (MnO_xCl_y).[32,44] This peak appeared due to the reaction between the absorbed Cl species with surface Mn during CB decomposition, which was in agreement with the Raman result.

For fresh Sn-MnCeLa, two broad overlapped reduction peaks of Mn appeared at around 350 °C and 460 °C, implying that the addition of Sn increased the difficulty of reducing the Mn species, which was consistent with the results of Corradini and co-workers[45] and Raman. Moreover, the TPR profile of fresh Sn-MnCeLa showed a peak with a maximum at approximately 540 °C, which was attributed to the reduction of SnO_2,[21] i.e., $Sn^{4+} \rightarrow Sn^{2+}$ and $Sn^{2+} \rightarrow Sn^0$. For the used samples, the TPR reduction peaks corresponding to the Mn species followed a nearly similar pattern as those for the fresh Sn-MnCeLa catalyst. On the other hand, the TPR peaks of the MnO_x were less intense compared with those of fresh MnCeLa, indicating that Mn existed mainly in low valence

state, which was in accord with the XPS results. In addition, no reduction peaks were observed in the region of 700-800 °C for the used Sn-MnCeLa catalysts, indicating that Sn doping could inhibit the formation of MnO_xCl_y.

3.4. Reaction mechanism

In the catalytic oxidation of CB, the CB molecule is adsorbed and dissociated on MnO_x active sites via nucleophilic attacks on C-Cl bond.[46,47] Subsequently, the dissociated CB can be easily completely oxidized into H_2O and CO_2 by active oxygen species. Simultaneously, the dissociative Cl species adsorbed on the metal cation (i.e., Mn^{X+} or Sn^{X+}) are oxidized into Cl_2 by surface reactive oxygen species. However, the removal of Cl species from the active sites of Mn-based catalysts is considerably more difficult, which requires enough surface reactive oxygen species. According to the XPS results, the doping of Sn can significantly increase the concentration of the surface adsorbed oxygen, which is used for Deacon Process. On the other hand, the addition of Sn inhibits the formation of MnO_xCl_y, avoiding MnCeLa catalyst deactivating. These two aspects are the reasons for the enhanced resistance to chlorine poisoning of Sn modified MnCeLa catalysts. According to the analysis above, a plausible reaction mechanism can be proposed for the catalytic combustion of CB over Mn-based and Sn doped Mn-based catalysts as shown in Scheme 1.

4. Conclusions

In summary, it has been found that both MnCeLa and SnMnCeLa mixed oxide catalysts prepared by sol-gel and coprecipitation method exhibited high activity for the low temperature catalytic destruction of CB, whereas the Sn-MnCeLa catalysts showed significantly higher stabilities than that of the MnCeLa catalysts. At 250 °C, Sn-MnCeLa showed more stable activity

with a conversion of greater than 95% during the 30 h reaction than all reported catalysts for CB oxidation, implying that the addition of Sn could remarkably improve the stability of MnCeLa catalysts for chlorobenzene oxidation. The characterization results revealed that the enhanced stability of the Sn-MnCeLa catalysts can be attributed to the fact that the addition of Sn could increase the concentration of surface adsorbed oxygen species for removal of the adsorbed Cl species and inhibit the formation of MnO_xCl_y, avoiding the deactivation of the MnCeLa catalyst. Therefore, the Sn-modified MnCeLa catalyst appears to be a promising candidate in the abatement of CVOCs at low-temperatures.

Acknowledgement

This work was financially supported by the National Natural Science Foundation of China (No. 20873097, 21071113, 21471120), Natural Science Foundation of Hubei Province (No. 2011CDA049), International Cooperation Foundation of Hubei Province (2012IHA00201).

References

1 M. J. Morra, V. Borek and J. Koolpe, *J. Environ. Qual.*, 2000, **29**,706-715.

2 H. Kominami, T. Nishi, K. Fuku and K. Hashimoto, *RSC Adv.*, 2013, **3**, 6058-6064.

3 N. Li and F. Gaillard, *Appl. Catal., B*, 2009, **88**, 152-159.

4 J. Johnson, Environ. *Sci.Technol.*, 1995, **29**, 24a-32a.

5 Y. Liu, Z. B. Wei, Z. C. Feng, M. F. Luo, P. L. Ying and C. Li, *J. Catal.*, 2001, **202**, 200-204.

6 W. Tian, H. S. Yang, X. Y. Fan and X. B. Zhang, *Catal. Commun.*, 2010, **11**, 1185-1188.

7 W. Tian, X. Y. Fan, H. S. Yang and X. B. Zhang, *J. Hazard. Mater.*, 2010, **177**, 887-891.

8 A. Jha, T. Chandole, R. Pandya, H. S. Roh and C. V. Rode, *RSC Adv.*, 2014, **4**, 19450-19455.

9 H. S. Liang, H. C. Wang and M. B. Chang, *Ind. Eng. Chem. Res.*, 2011, **50**, 13322-13329.

10 P. Zhao, C. N. Wang, F. He and S. T. Liu, *RSC Adv.*, 2014, **4**, 45665-45672.

11 X. Y. Wang, Q. Kang and D. Li, *Appl. Catal., B*, 2009, **86**, 166-175.

12 Y. Dai, X. Y. Wang, D. Li and Q. G. Dai, *J. Hazard. Mater.*, 2011, **188**, 132-139.

13 Y. J. Lu, Q. G. Dai and X. Y. Wang, *Catal. Commun.*, 2014, **54**, 114-117.

14 N. López, J. Gómez-Segura, R. P. Marín and J. Pérez-Ramírez, *J. Catal.*, 2008, **255**, 29-39.

15 C. Mondelli, A. P. Amrute, F. Krumeich, T. Schmidt and J. Pérez-Ramírez, *Chem. Cat. Chem.*, 2011, **3**, 657-660.

16 A. Iglesias-González, J. L. Ayastuy , M. P. González-Marcos and M. A. Gutiérrez-Ortiz, *Int. J . Hydrogen. Energ.*, 2014, **39**, 5213-5224.

17 R. Sasikala, N. M. Gupta and S. K. Kulshreshtha, *Catal. Lett.*, 2001, **71**, 69-73.

18 X. L. Li, Y. H. Li, S. S. Deng and T. A. Rong, *Catal. Commun.*, 2013, **40**, 47-50.

19 J. L. Ayastuy, M. P. González-Marcos and M. A. Gutiérrez-Ortiz, *Catal. Commun*., 2011, **12**, 895-900.

20 H. Z. Chang, X. Y. Chen, J. H. Li, L. Ma, C. Z. Wang, C. X. Liu, J. W. Schwank and J. M. Hao, *Environ. Sci. Technol.*, 2013, **47**, 5294-5301.

21 H. Z. Chang, J. H. Li, X. Y. Chen, L. Ma, S. J. Yang, J. W. Schwank and J. M. Hao, *Catal. Commun.*, 2012, **27**, 54-57.

22 Y. Dai, X. Y. Wang, Q. G. Dai and D. Li, *Appl. Catal., B*, 2012, **111-112**, 141-149.

23 Y. J. Lu, Q. G. Dai and X. Y. Wang, *Catal. Commun.*, 2014, **54**, 114-117.

24 M. Wu, X. Y. Wang, Q. G. Dai, Y. X. Gu and D. Li, *Catal. Today*, 2010, **158**, 336-342.

25 H. Yoshihito and A. Akimi, *Appl. Catal., A*, 2003, **250**, 247-254.

26 J. M. Giraudon, A. Elhachimi and G. Leclercq, *Appl. Catal., B*, 2008, **84**, 251-261.

27 A. Aznárez, R. Delaigle, P. Eloy, E. M. Gaigneaux, S. A. Korili and A. Gil, *Catal. Today*, 2014, DOI: 10.1016/manuscript number.

28 X. R. Zeng, R. B. Zhang, X. L. Xu and X. Wang, *J. Rare Earth*, 2012, **30**, 1013-1019.

29 J. W. Li, P. Zhao and S. T. Liu, *Appl. Catal., A*, 2014, **482**, 363-369.

30 F. Arena, G. Trunfio, J. Negro, B. Fazio and L. Spadaro, *Chem.Mater.*, 2007, **19**, 2269-2276.

31 A. Bueno-López, K. Krishna, M. Makkee and J. A. Moulijn, *J. Catal.*, 2005, **230**, 237-248.

32 Y. Liu, M. F. Luo, Z. B. Wei, Q. Xin, P. L. Ying and C. Li, *Appl. Catal., B*, 2001, **29**, 61-67.

33 F. Buciuman, F. Patcas, R. Craciun and D. R. T. Zahn, *Phys. Chem. Chem. Phys.*, 1999, **1**, 185-190.

34 L. Abello, B. Bochu, A. Gaskov, S. Koudryavtseva, G. Lucazeau and M. Roumyantseva, *J. Solid State Chem.*, 1998, **135**, 78-85.

35 X. F. Tang, J. H. Li, L. S. Wei and J. M. Hao, *Chin. J. Catal.*, 2008, **29**, 531-536.

36 B. X. Shen, X. P. Zhang, H. Q. Ma, Y. Yao and T. Liu, *J. Enviro. Sci.*, 2013, **25**, 791-800.

37 Y. Liu, W. C. Wu, Y. J. Guan, P. L. Ying and C. Li, *Langmuir*, 2002, **18**, 6229-6232.

38 Q. G. Dai, S. X. Bai, X. Y. Wang and G. Z. Lu, *Appl. Catal., B*, 2013, **129**, 580-588.

39 D. R. Mullins, S. H. Overbury and D. R. Hunteley, *Surf. Sci.*, 1998, **409**, 307-319.

40 X.Y. Fan, H. S. Yang, W. Tian, A. M. Nie, T. F. Hou, F. M. Qiu and X. B. Zhang, *Catal. Lett.*, 2011, **141**, 158-162.

41 F. Kapteijn, L. Singoredjo, A. Andreini and J. A. Moulijn, *Appl. Catal., B*, 1994, **3**, 173-189.

42 J. Trawczyński, B. Bielak and W. Miśta, *Appl. Catal., B*, 2005, **55**, 277-285.

43 J. Carnö, M. Ferrandon, E. Björnbom and S. Järås, *Appl. Catal., A*, 1997, **155**, 265-281.

44 D. Döbber, D. Kießling, W. Schmitz and G. Wendt, *Appl. Catal., B*, 2004, **52**, 135-143.

45 S. A. da S. Corradini, G. G. Lenzi, M. K. Lenzi, C. M. F. Soares and O. A. A. Santos, *J. Non-Cryst. Solids*, 2008, **354**, 4865-4870.

46 L. Janine and M. D. Amiridis, *J. Catal.*, 2004, **223**, 296-308.

47 C. E. Hetrick, L. Janine and M. D. Amiridis, *Appl. Catal., B*, 2008, **77**, 255-263

Figure captions

Table 1 Physical properties and XPS data of MnCeLa and Sn-MnCeLa catalysts.

Fig. 1 The activity of SnO_2, MnCeLa and Sn-MnCeLa catalysts for CB combustion. Reaction conditions: 200 mg samples, 2500 mg/m^3 CB, 20% O_2, N_2 balance; GHSV = 20,000 h^{-1}.

Fig. 2 The stabilities of MnCeLa and Sn(0.08)-MnCeLa catalysts for CB combustion at different temperatures: a) 200 °C; b) 225 °C; c) 250 °C; d) 275 °C; e) 300 °C; gas composition: 2500 mg/m^3 CB, 20% O_2, N_2 balance; GHSV = 20,000 h^{-1}.

Fig. 3 XRD patterns of MnCeLa and Sn-MnCeLa catalysts before and after CB oxidation: used MnCeLa and Sn-MnCeLa represent catalysts reacted at 200 °C for 30 h.

Fig. 4 Raman spectra of MnCeLa and Sn-MnCeLa catalysts before and after CB oxidation.

Fig. 5 Mn 2p (A), O 1s (B), Sn 3d (C) and Cl 2p (D) XPS spectra of MnCeLa and Sn-MnCeLa catalysts: a, fresh MnCeLa; b, used MnCeLa; c, fresh Sn-MnCeLa; d, used Sn-MnCeLa.

Fig. 6 H_2-TPR profiles of MnCeLa (A) and Sn-MnCeLa (B) catalysts: fresh represents fresh catalysts; 225 °C, 250 °C, 275 °C and 300 °C represent the catalysts reacted at corresponding temperatures for 30 h, respectively, and denoted as MnCeLa(X) or Sn-MnCeLa(X) in the text, i.e., MnCeLa (275◦C).

Scheme 1 The proposed reaction mechanism for the catalytic combustion of CB over Mn-based and Sn doped Mn-based catalysts.

Table 1

Physical properties and XPS data of MnCeLa and Sn-MnCeLa catalysts.

Catalysts	Surface area (m^2/g)[a]	Pore volume ($\times 10^{-2} cm^3/g$)	Average pore (nm)	Mn (at.%)			O (at.%)		Sn (at.%)	
				Mn^{4+}	Mn^{3+}	Mn^{2+}	O_{ads}	O_{latt}	Sn^{4+}	Sn^{2+}
Fresh MnCeLa	75	21.09	5.04	26.2	39.6	34.2	21.9	78.1	-	-
Used MnCeLa	55	20.43	5.26	15.9	47.0	37.1	12.8	87.2	-	-
Fresh Sn-MnCeLa	93	26.41	5.10	35.2	47.1	17.7	30.2	69.8	70.1	29.9
Used Sn-MnCeLa	62	25.98	5.27	30.7	45.5	23.8	17.6	82.4	63.8	36.2

[a] The specific surface area is calculated using the BET model.

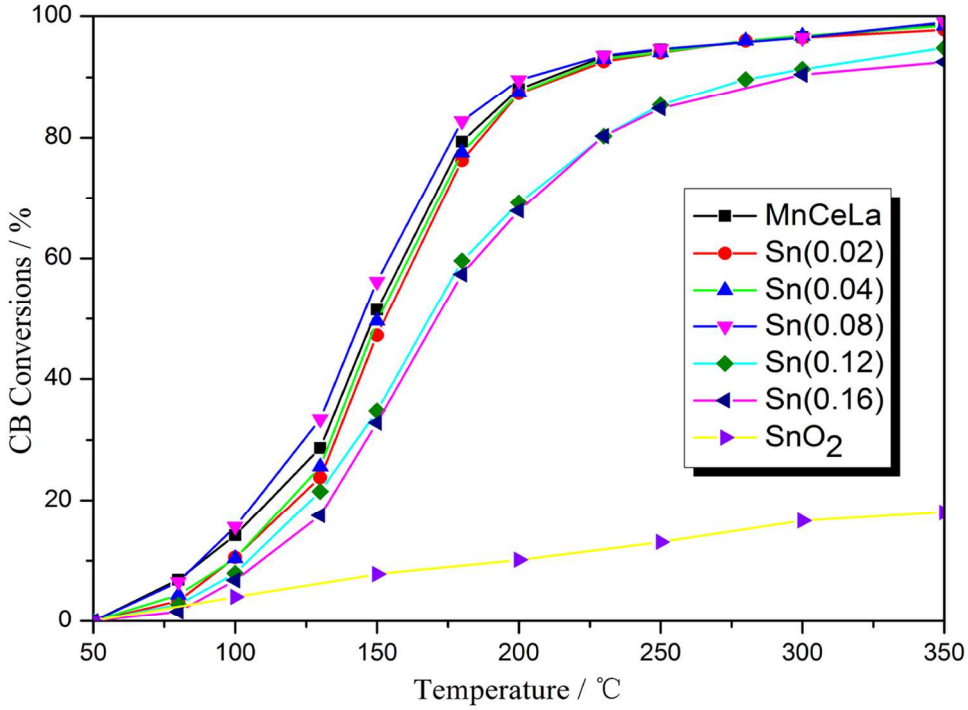

Fig. 1 The activity of SnO2, MnCeLa and Sn-MnCeLa catalysts for CB combustion. Reaction conditions: 200 mg samples, 2500 mg/m3 CB, 20% O2, N2 balance; GHSV = 20,000 h-1.
60x43mm (600 x 600 DPI)

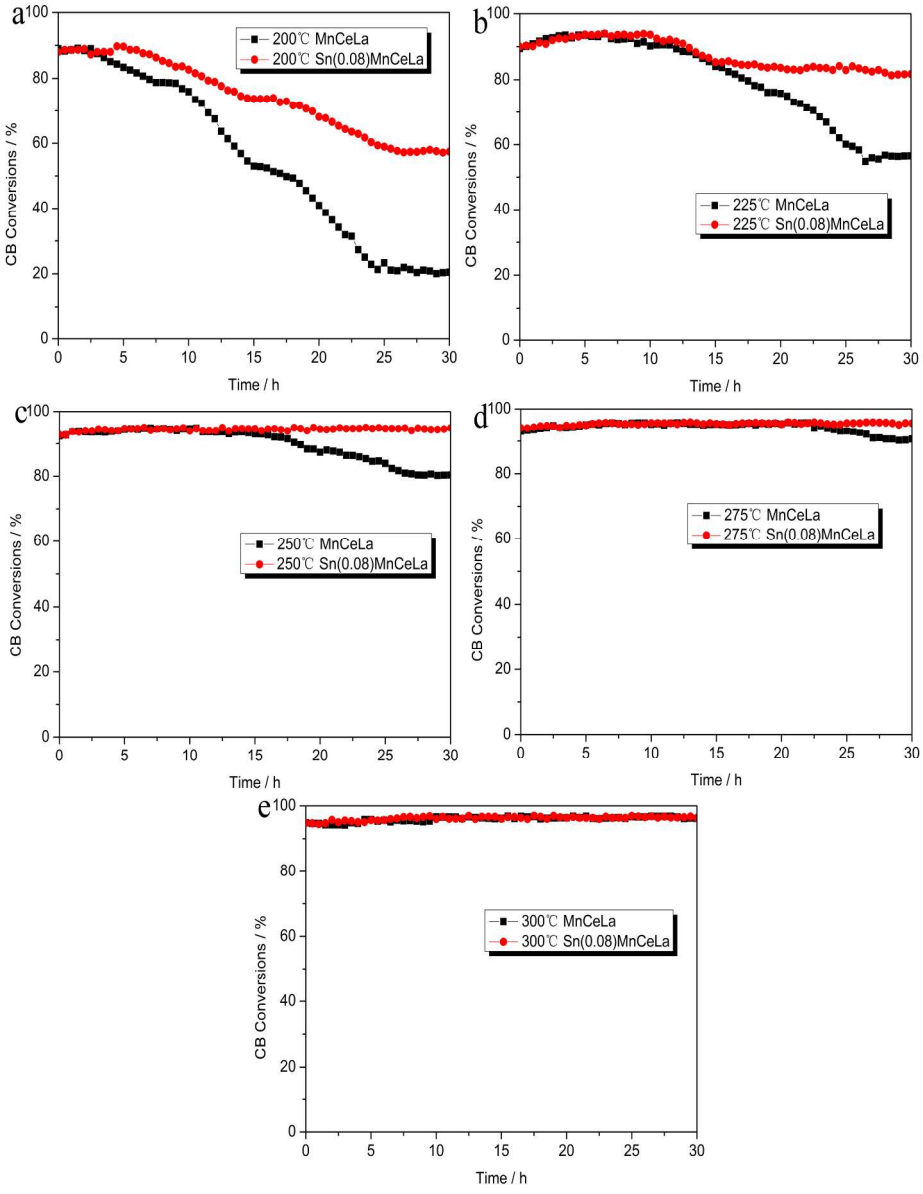

Fig. 2 The stabilities of MnCeLa and Sn(0.08)-MnCeLa catalysts for CB combustion at different temperatures: a) 200 °C; b) 225 °C; c) 250 °C; d) 275 °C; e) 300 °C; gas composition: 2500 mg/m3 CB, 20% O2, N2 balance; GHSV = 20,000 h-1.
219x283mm (300 x 300 DPI)

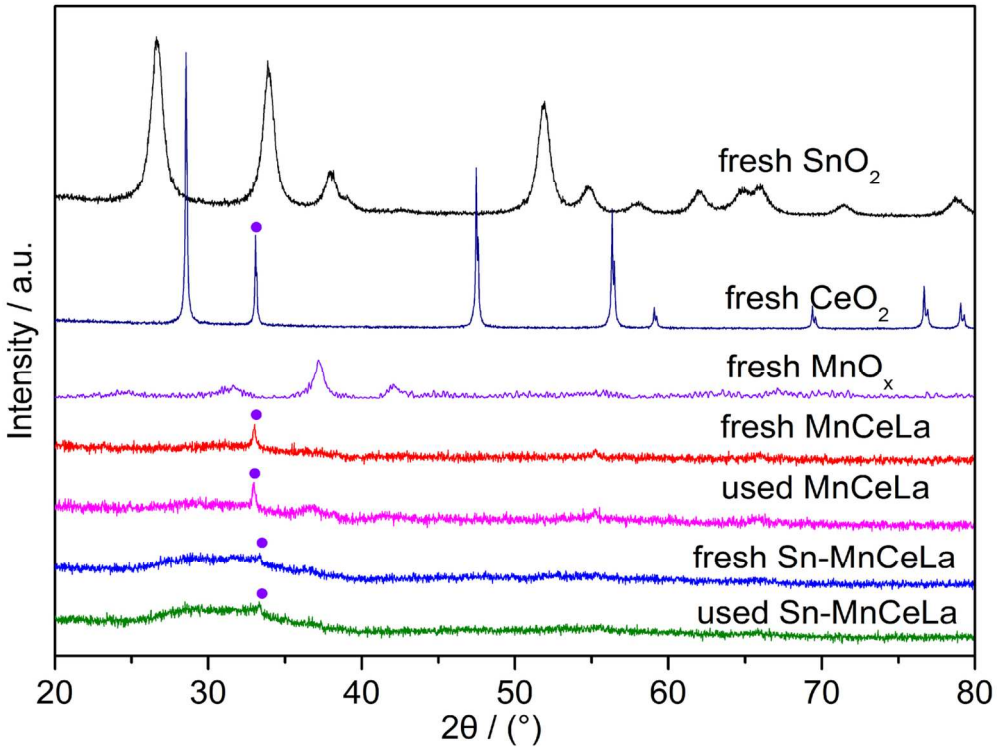

Fig. 3 XRD patterns of MnCeLa and Sn-MnCeLa catalysts before and after CB oxidation: used MnCeLa and Sn-MnCeLa represent catalysts reacted at 200 °C for 30 h.
62x47mm (600 x 600 DPI)

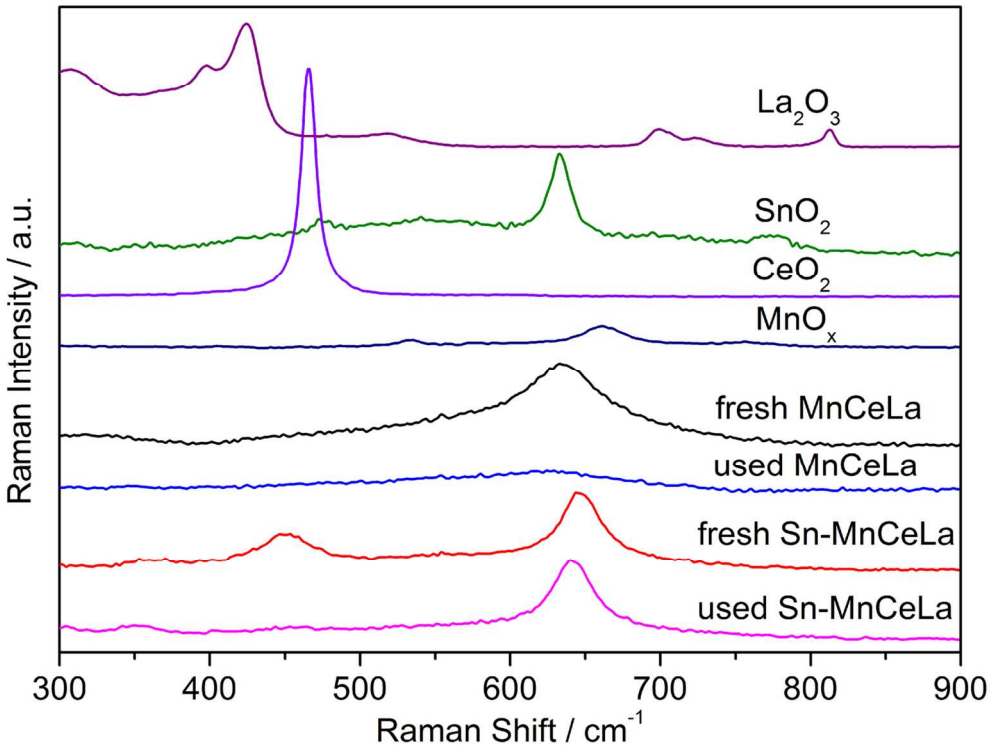

Fig. 4 Raman spectra of MnCeLa and Sn-MnCeLa catalysts before and after CB oxidation.
62x47mm (600 x 600 DPI)

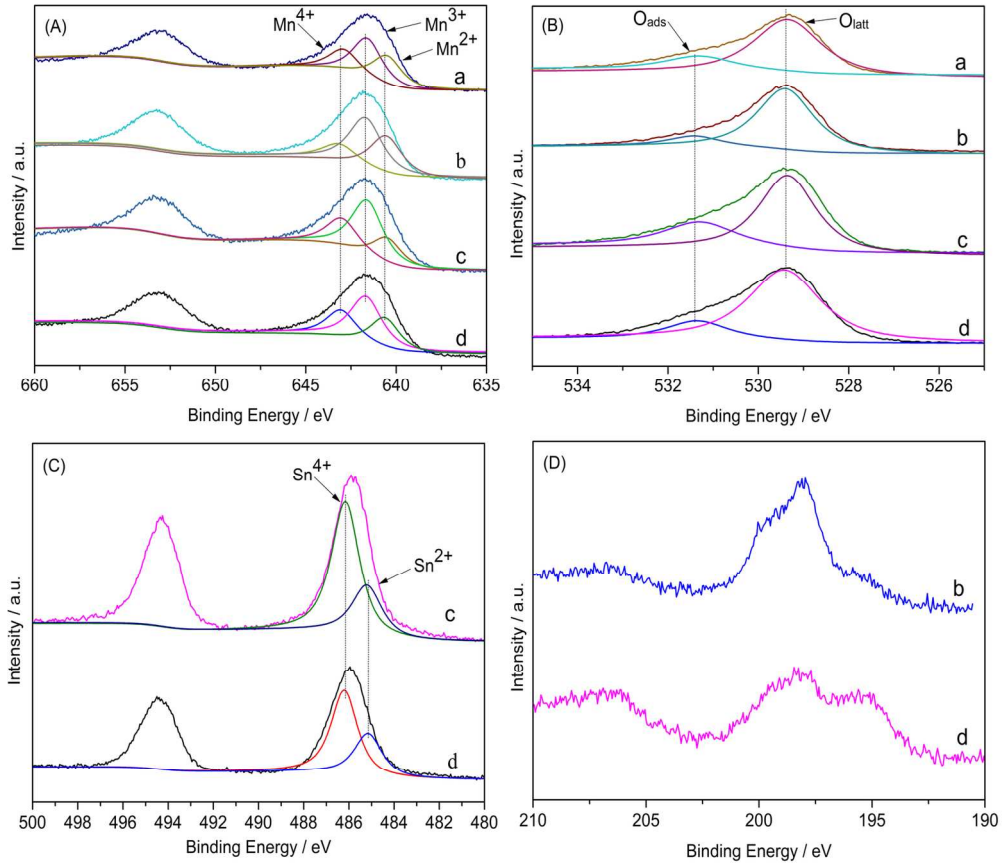

Fig. 5 Mn 2p (A), O 1s (B), Sn 3d (C) and Cl 2p (D) XPS spectra of MnCeLa and Sn-MnCeLa catalysts: a, fresh MnCeLa; b, used MnCeLa; c, fresh Sn-MnCeLa; d, used Sn-MnCeLa.
149x131mm (300 x 300 DPI)

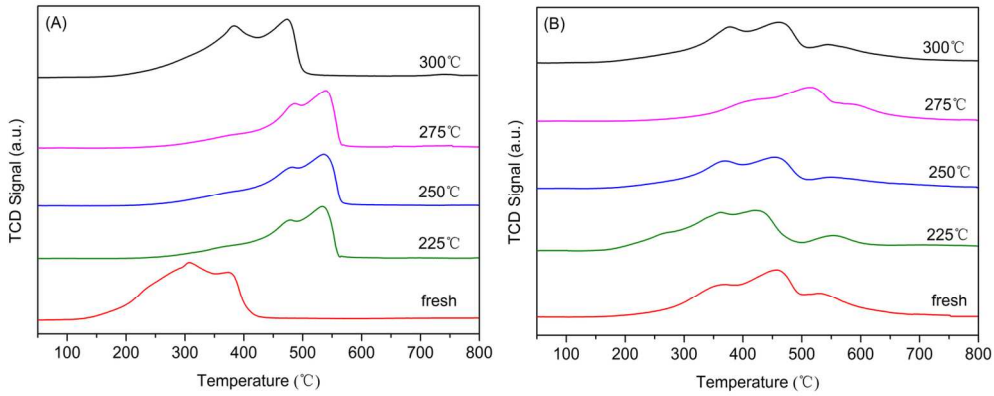

Fig. 6 H2-TPR profiles of MnCeLa (A) and Sn-MnCeLa (B) catalysts: fresh represents fresh catalysts; 225 °C, 250 °C, 275 °C and 300 °C represent the catalysts reacted at corresponding temperatures for 30 h, respectively, and denoted as MnCeLa(X) or Sn-MnCeLa(X) in the text, i.e., MnCeLa (275◦C).
69x28mm (600 x 600 DPI)

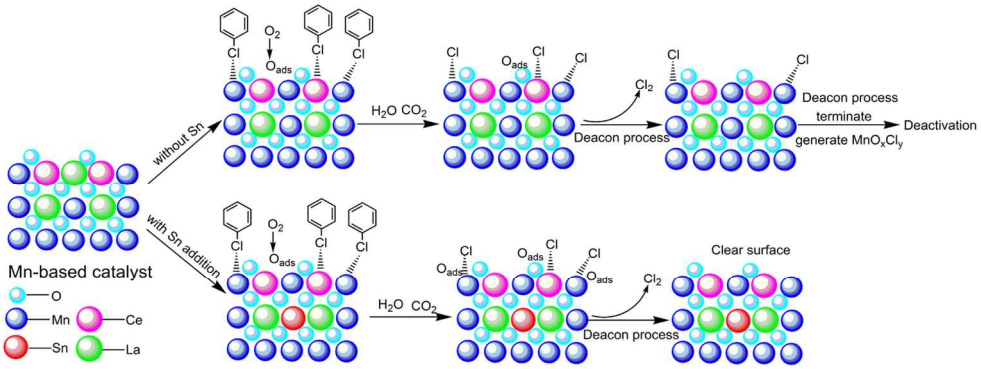

Scheme 1 The proposed reaction mechanism for the catalytic combustion of CB over Mn-based and Sn doped Mn-based catalysts.
64x24mm (600 x 600 DPI)